JOURNAL OF SOLID STATE CHEMISTRY 91, 225–237 (1991)

Synthesis, Crystal Structure, and Properties of Metallic $PrNiO_3$: Comparison with Metallic $NdNiO_3$ and Semiconducting $SmNiO_3$

P. LACORRE,*,† J. B. TORRANCE,* J. PANNETIER,‡ A. I. NAZZAL,* P. W. WANG,* AND T. C. HUANG*

IBM Research Division, Almaden Research Center, 650 Harry Road, San Jose, California 95120-6099; and ‡Institut Laue Langevin, 156X, 38042 Grenoble, Cedex, France

Received August 29, 1990

The compound $PrNiO_3$ has been prepared for the first time. Using only moderate oxygen pressure, $PrNiO_3$, $NdNiO_3$, and $SmNiO_3$ were made and found to crystallize in the $GdFeO_3$—type orthorhombically distored perovskite structure. Structural refinements for all three compounds reveal NiO_6 octahedra with an average Ni–O distance of 1.94–1.95 Å, about the same as in the more distorted $HoNiO_3$. The electrical conductivity of $PrNiO_3$ is metallic at room temperature, but undergoes a transition at 130 K to an insulating state. Examination of the conductivities of the corresponding Sm, Nd, and La compounds reveals a monotonic pattern of behavior: as the rare earth radius is increased, the compounds become more conducting because the metal–insulator transition temperature decreases from 400 K(Sm) to 200 K(Nd) to 130 K(Pr) to none for La. From DSC and lattice constant measurements, this transition is shown to be first order, with a ~0.2% contraction upon heating into the metallic state. Low temperature neutron measurements in the insulating phase reveal new diffraction peaks, probably related to magnetic ordering of Ni and/or *RE* moments.

Introduction

Since the discoveries (*1–3*) of superconductivity at anomalously high temperatures in a series of bismuth oxides and copper oxides, there is renewed interest in other oxide systems, particularly those which exhibit high electrical conductivity. This interest is partially fueled by the hope that the study of other oxides will give insight which may significantly contribute to the understanding of the superconducting oxides. Although metallic conductivity is relatively rare in oxides (*4, 5*), it has been observed (*6*) in $LaNiO_3$, even without doping. We report here a study of the synthesis and properties of three other members of the series *RE*-NiO_3, namely *RE* = Sm, Nd, and (for the first time) Pr. In addition, the room temperature crystal structure has been determined for $PrNiO_3$ from neutron and X-ray power diffraction and for $NdNiO_3$ and $SmNiO_3$ from X-rays alone.

In general, the preparation of $RENiO_3$ involves the following reaction:

$$RE_2O_3 + 2NiO + \tfrac{1}{2}O_2 \rightarrow RENiO_3$$

Since it is somewhat difficult to oxidize

† Permanent address: Laboratoire des Fluorures, Faculté des Sciences, Université du Maine, 72017 Le Mans, Cedex, France.

0022-4596/91 $3.00

nickel to Ni(III), this reaction does not proceed at low oxygen pressures ($P(O2) \leq 1$ bar) or at the high temperatures (800–1000°C) usually needed for solid state reactions. Thus, two general strategies have been adopted: carry out the reaction at higher oxygen pressures or at lower temperatures. The latter approach was first used by Wold *et al.* (*7*) to prepare $LaNiO_3$ at 600°C, with the aid of a $NaCO_3$ flux. Recently, Vassiliou *et al.* (*8*) have prepared $NdNiO_3$ at 650°C and 1 atm of oxygen, starting with nitrates or a sol gel. In contrast, Demazeau *et al.* (*9*) used 60 K bar of oxygen pressure to help stabilize Ni(III) at 950°C. Using oxides as starting materials and $KClO_3$ as an oxygen source, they were able to prepare salts with Y and all of the rare earths (*RE*), except Ce, Pr, and Tb. In this paper, we show that, starting with nitrates, the compounds with *RE* = La, Pr, Nd, and Sm can be prepared at 1000°C with the more readily attainable pressures of 150–200 bar of oxygen. The preparation of $PrNiO_3$ has not been reported previously.

Experimental

Sample Preparation and Physical Measurements

The $RENiO_3$ polycrystalline samples were synthesized from a fine and intimate mixture of oxides obtained from the decomposition of the corresponding nitrates. The nitrates were synthesized by dissolution of a stoichiometric mixture of the elementary oxides in a solution of nitric acid, and then drying the solution. After decomposition of the residue at about 200–300°C, this intimate mixture of oxides was fired at 600°C for several hours and pressed into pellets. The pellets were then fired at 1000°C for several days under 150–200 bars of oxygen with several intermediate regrindings and repressings. The resulting samples were dark brown to black in color.

The DSC measurements were made on a DuPont Differential Scanning Calorimeter (Model 910) in the temperature range 110–860 K on samples weighing ~40 mg. For full range scans, heating rates of 20°C/min were applied. Slower scans of 5°C/min were used around the transition to determine the values of the change in enthaply. Conductivity measurements were carried out using the conventional four-probe technique in the range 5–450 K with a cooling rate of about 10–20°C/min. Further measurements with much slower heating/cooling rates (≈1°C/min) were made on $PrNiO_3$ and $NdNiO_3$ around the transition to measure the hysteresis.

X-Ray and Neutron Diffraction

X-ray diffraction patterns were collected at room temperature on a modified vertical θ–2θ scanning Norelco diffractometer ($PrNiO_3$) and on a D500 Siemens diffractometer ($NdNiO_3$, $SmNiO_3$), both using Cu$K\alpha$ radiation. For the structure determinations, diffraction patterns were recorded in the 2θ ranges 20–160° (step $\Delta 2\theta = 0.025°$) for $PrNiO_3$, 18–150° (step $\Delta 2\theta = 0.020°$) for $NdNiO_3$ and 20–150° (step $\Delta 2\theta = 0.020°$) for $SmNiO_3$.

Neutron diffraction data were collected on the powder diffractometers D20 and D1B of the High Flux Reactor of the Institut Laue Langevin (Grenoble, France). The room temperature structure of $PrNiO_3$ was refined from a pattern collected on the two-axis powder diffractometer D20. The instrument was used in its high resolution mode (primary collimation $\alpha_1 = 10'$). The 126-cell position-sensitive detector was used in the scanning mode in the angular range $4° < 2\theta < 150°$. The 2.416 Å neutron beam provided by a vertically focusing highly oriented pyrolytic graphite (HOPG) monochromator was filtered to remove higher order contamination. The sample was packed in a 7-mm diameter vanadium can held within a vacuum vessel. The full pattern was collected over a period of about 140 min.

The low temperature neutron thermodiffractometry was performed on the high flux powder diffractometer D1B using a wavelength of 2.52 Å. The samples were contained in a vanadium can (ϕ = 10 mm, h = 50 mm) held in a standard helium cryostat. For the temperature scan, the 400-cell position-sensitive detector was set to the angular range $5° < 2\theta < 85°$. For $PrNiO_3$ and $NdNiO_3$, 4-min diffraction patterns were recorded every 1.0 and 1.3 K, respectively, from 1.2 to ~300 K. The fitting of the reflection positions and intensities versus temperature in the neutron thermodiffractometry was done using the program ABFfit (*10*). All other X-ray and neutron data analysis were performed with a modified version (*11*) of the multipattern Rietveld code distributed by R. A. Young (*12*). Line shapes were approximated by a pseudo-Voïgt function. Neutron wavelengths have been calibrated with respect to the X-ray determined room temperature cell parameters of $PrNiO_3$.

Lattice Constants of $RENiO_3$

The X-ray powder diffraction patterns of the four $RENiO_3$ salts prepared are shown in Fig. 1. They appear single phase, with the exception of a small amount of NiO observable in some preparations. These patterns have been indexed in the same space group (*13*) (*Pbnm*) as $GdFeO_3$ and the resulting lattice constants are tabulated in Table I and plotted in Fig. 2, along with other data (*8, 9*) for $RENiO_3$.

Our results are best discussed in the context of the general features of perovskite materials (*4*). The crystal structure of a number of $REMO_3$ perovskite structures have been reported previously. The structures contain an array of corner sharing MO_6 octahedra which may be approximated as undistorted, with a metal oxygen distance d_{M-O} that is independent of the rare earth (*RE*). In the ideal perovskite structure, these octahedra sit at the corners of a cubic unit cell, with their axes oriented along the cell edges. In the center, there is space for the *RE* ion, which will fit perfectly if $d_{RE-O} = \sqrt{2}d_{M-O}$. Since the *RE* are too small to satisfy this criterion, the MO_6 octahedra are tilted and rotated to fill the extra space around the rare earth (*RE*) ion. These rotations cause the unit cell to be smaller and distorted from the ideal cubic cell. Since the magnitude of this distortion is related to the relative distances d_{M-O} and d_{RE-O}, it may be discussed in terms of a tolerance factor (*14*) defined as $t = d_{RE-O}/\sqrt{2}\, d_{M-O}$. If cations *RE* and *M* could be found such that $t = 1$, presumably they would form the ideal cubic perovskite structure. For those with t slightly less than 1, the MO_6 octahedra are observed to be rotated about the (111)-axis, giving rise to a rhombohedral unit cell, such as in $LaNiO_3$ (*7*). For smaller t, the octahedra tilt about (110) and (001), resulting in the orthorhombic $GdFeO_3$ structure (*13*). For still smaller values of t, other, nonperovskite structures become favored.

There are a number of possible sources of estimated values for d_{RE-O} and d_{M-O}. For the former, we have chosen to take those of Poix (*15*), who has collected a complete set of d_{RE-O} for 12-coordinated *RE*. For d_{M-O} we have taken the experimental values found in perovskite structures (rather than those found in M_2O_3, MCl_3, etc.). For Ni, a value of d_{M-O} = 1.94 Å is obtained from the structure (*9*) of $HoNiO_3$ and from our refinement of the Pr and Nd structures (see below). The ideal undistorted, cubic perovskite would then have a lattice constant a_p = 3.88 Å. Using these values to determine t for a large number of $REMO_3$ compounds, we show the dependence of the structure on t at the top of Fig. 2. There is a well-defined boundary at t = 0.985 above which rhombohedral structures are formed and below which the atoms form an orthorhombic structure.

We can see from Fig. 2 that $NdNiO_3$ and $PrNiO_3$ are orthorhombic, but rather near the boundary between orthorhombic and

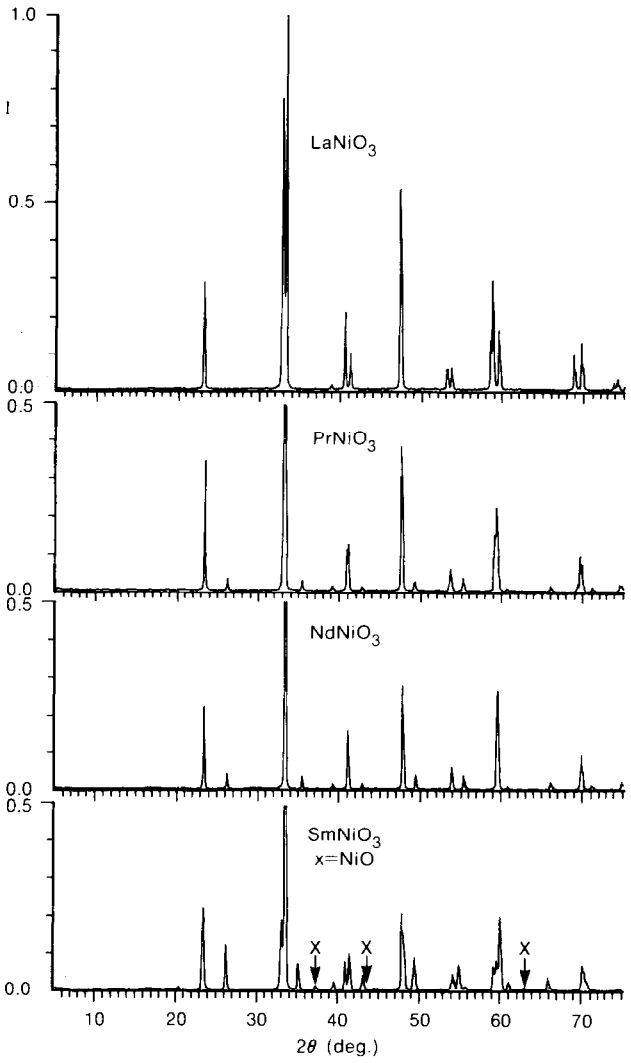

FIG. 1. Comparison of X-ray powder diffraction patterns of $RENiO_3$.

rhombohedral structures. At high temperatures, some orthorhombic compounds have been found (*16*) to have a reversible transition to a rhombohedral phase. For example, $LaCrO_3$ has such a transition (*17*) near 540 K. Differential scanning calorimetric measurements on $PrNiO_3$ reveal a first-order phase transiton at 780 K, whereas no transition was found in the Nd compound up to 870 K. In the Pr compound, X-ray powder diffraction measurements demonstrate that the structure above this transition is rhombohedral, as discussed in more detail elsewhere (*18*).

The characteristic splitting of the X-ray peaks evident in the $LaNiO_3$ pattern (Fig. 1) is indicative of the rhombohedral distortion in this structure, while the presence of additional peaks (near 26°, 35°, and 49°, for example) in the Pr, Nd, and Sm compounds

TABLE I

ROOM TEMPERATURE X-RAY LATTICE PARAMETERS OF $RENiO_3$

RE	La		Pr	Nd			Sm	
t	0.987		0.976	0.972			0.965	
structure	Rhombohedral	Rhombohedral	Orthorhombic	Rhombohedral	Orthorhombic	Orthorhombic	Orthorhombic	Orthorhombic
a(Å)	5.393	5.3954	5.4154	5.40	5.384	5.3888	5.336	5.3283
b(Å)			5.3755		5.384	5.3845	5.431	5.4374
c(Å)			7.6192		7.615	7.6127	7.568	7.5675
α_{rh}(°)	60.80	60.78		60.5				
Ref.	[a]	This work	This work	[b]	[a]	This work	[a]	This work

[a] From Ref. (9).
[b] From Ref. (8).

demonstrate the orthorhombic distortions of their unit cells. Note that the unit cell dimensions of $NdNiO_3$ (Table I and Fig. 2) satisfy almost exactly the condition $a \approx b \approx c/\sqrt{2} \approx 5.40$ Å, as noted earlier (*9*). Nevertheless, the extra peaks observed in the pattern clearly indicate that the crystal structure is orthorhombic, as does the fact that this pseudocubic lattice constant (3.807 Å) is much smaller than the value $a_p = 3.88$ Å expected for the ideal cubic perovskite.

Recently, a new form of $NdNiO_3$ has been isolated (*8*) and indexed to a rhombohedral unit cell. This new form, hereafter called *RH*-$NdNiO_3$, was synthesized at $P(O_2) = 1$ bar at $T = 650$°C, in contrast to the condi-

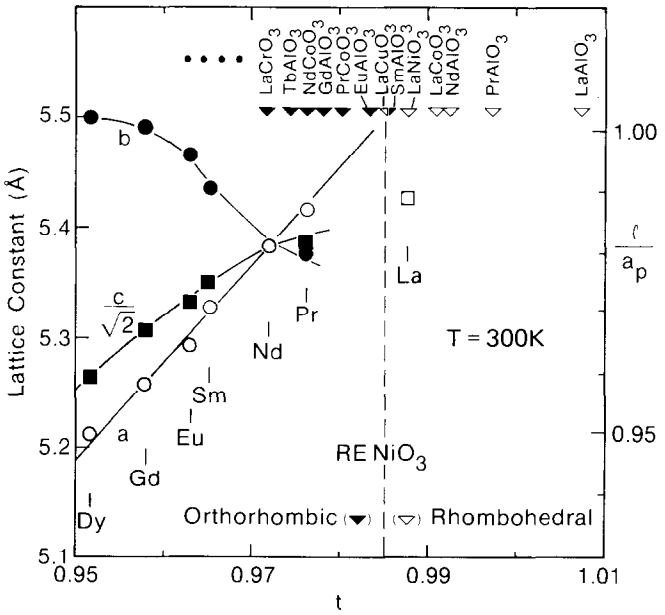

FIG. 2. Dependence on tolerance factor of lattice constants of $RENiO_3$ compounds and orthorhombic or rhombohedral structure of $REMO_3$ compounds, showing boundary between these two phases near $t = 0.985$. (l/a_p represents the ratio of the lattice constant value to the lattice constant of an ideal cubic perovskite.)

TABLE II

ROOM TEMPERATURE STRUCTURAL PARAMETERS FOR ORTHORHOMBIC $RENiO_3$

	$PrNiO_3$		$NdNiO_3$	$SmNiO_3$	$HoNiO_3$[a]
	Neutron	X-ray	X-ray	X-ray	X-ray
a(Å)	5.4145(3)	5.4154(1)	5.3888(2)	5.3283(1)	5.181(2)
b(Å)	5.3753(2)	5.3755(1)	5.3845(1)	5.4374(1)	5.510(2)
c(Å)	7.6206(4)	7.6192(2)	7.6127(2)	7.5675(2)	7.425(3)
V(Å^3)	221.80(4)	221.80(2)	220.89(2)	219.25(2)	211.96(25)
RE					
x	0.9917(11)	0.9959(3)	0.9935(2)	0.9894(2)	0.981(1)
y	0.0310(7)	0.0293(2)	0.0359(1)	0.0514(1)	0.064(1)
z	1/4	1/4	1/4	1/4	1/4
B(Å^2)	−0.02(3)	0.09(2)	0.29(2)	0.28(1)	0.200(1)
Ni					
x	1/2	1/2	1/2	1/2	1/2
y	0	0	0	0	0
z	0	0	0	0	0
B(Å^2)	−0.02(3)	0.09(2)	0.29(2)	0.38(3)	1.00(2)
O1					
x	0.0652(8)	0.0739(24)	0.0743(29)	0.0951(16)	0.086(2)
y	0.4931(8)	0.4948(17)	0.4930(14)	0.4813(13)	0.464(1)
z	1/4	1/4	1/4	1/4	1/4
B(Å^2)	0.28(3)	0.09(2)	0.29(2)	0.18(9)	2.0(1)
O2					
x	0.7227(5)	0.7251(20)	0.7140(20)	0.7119(12)	0.708(1)
y	0.2833(4)	0.2829(19)	0.2879(19)	0.2890(12)	0.290(1)
z	0.0361(3)	0.0337(13)	0.0332(14)	0.0426(8)	0.047(1)
B(Å^2)	0.28(3)	0.09(2)	0.29(2)	0.18(9)	1.0(1)
R_F	0.020	0.033	0.043	0.033	0.080
R_{Bragg}	0.024	0.050	0.059	0.046	
R_P	0.044	0.118	0.082	0.083	
R_{WP}	0.057	0.150	0.119	0.108	

[a] From Ref. (*9*).

tions which yield the orthorhombic form: $P(O_2)$ = 150–200 bar at T = 1000°C (present work) and $P(O_2)$ = 60 kbar at 950°C (*9*). This orthorhombic phase, called *O*-$NdNiO_3$, has a more distorted structure with a smaller volume. The Ni–Ni distance for the latter is 3.81 Å compared with 3.85 Å for *RH*-$NdNiO_3$ and the value of 3.88 Å expected for the undistorted cubic perovskite. Perhaps the pressure during synthesis favors the smaller volume, orthorhombic phase. In this paper, we will continue to focus on the orthorhombic phase, *O*-$NdNiO_3$.

It should be noticed in Table II and Fig. 2 that the two smallest cell parameters are reversed in $PrNiO_3$ relative to the other orthorhombic members of the $RENiO_3$ series as given by Demazeau *et al.* (*9*). Such an inversion has already been noticed in other perovskites (*19–21*), such as $LaTiO_3$, $LaCrO_3$, and $LaGaO_3$ each with larger lanthanide cations compared to the other $RETiO_3$, $RECrO_3$, and $REGaO_3$, respectively. In *RE* NiO_3, the crossing point of the evolution of the cell parameters vs lanthanide corresponds almost exactly to *O*-$NdNiO_3$ (see Fig. 2). It is thus somewhat ambiguous to associate the amplitude of the orthorhombic

distortion with the splitting of the diffraction peaks. Even though $PrNiO_3$ exhibits a larger splitting than *O*-$NdNiO_3$, it is most probably less distorted than the latter. (This point is confirmed below.)

Crystal Structures of $RENiO_3$: *RE* = Pr, Nd, Sm

Full profile Rietveld structure refinements (*11*) of the room temperature X-ray diffraction patterns of $PrNiO_3$, $NdNiO_3$, and $SmNiO_3$ were carried out assuming the most common space group (*22*) for these distorted perovskites, that is *Pbnm*. Starting from a slight distortion of the perovskite lattice similar to that found (*9*) in $HoNiO_3$, the Rietveld algorithm quickly converges toward the structural parameters given in Table II. The weak scattering of X-rays from the oxygen ions relative to the nickel and praseodymium cations induced us to carry out a structural refinement from a neutron diffraction pattern in order to precisely locate the oxygen atoms. Because of the strong peak overlap in *O*-$NdNiO_3$ and the large absorption coefficient of Sm for neutrons, we have focused on $PrNiO_3$ only. The results of this refinement are given in Table II and differ only slightly from the X-ray diffraction results. The crystal structure of $PrNiO_3$ is illustrated in Fig. 3, while Table III gives the list of interesting interatomic distances and angles.

Compared to the other members of the series, the interpretation of $PrNiO_3$ is complicated by the two possible valence states of praseodymium (3+ and 4+). Significant amounts of Pr^{4+} would considerably reduce the *RE*–O distance and hence the tolerance factor, compared with the value of Poix (*15*) for Pr^{3+} used in Fig. 2. However, the data for $PrNiO_3$ behave as if the trivalent tolerance factor is appropriate: the *c*-axis lattice constant lies on the curve extrapolated from the other *RE* (Fig. 2), as does the temperature of the metal–insulator transition (see below). The structural transition from orthorhombic to rhombohedral found (*18*) at 780 K (above) also indicates that $PrNiO_3$ lies near the boundary at $t = 0.985$ in Fig. 2. As an additional check, we have used bond-valence theory (*23*) in order to get a measure of the charge on the Pr site. From the bond valence parameters for trivalent Pr, the calculated charge on the site is +3.12, very close to the ideal value of +3.0. A better agreement can be obtained by assuming a small (~7%) amount of Pr^{4+}, but the uncertainty is considerable. Based on the above considerations, we conclude that the Pr ion in $PrNiO_3$ is primarily Pr^{3+} with little (<10%), if any, Pr^{4+} present.

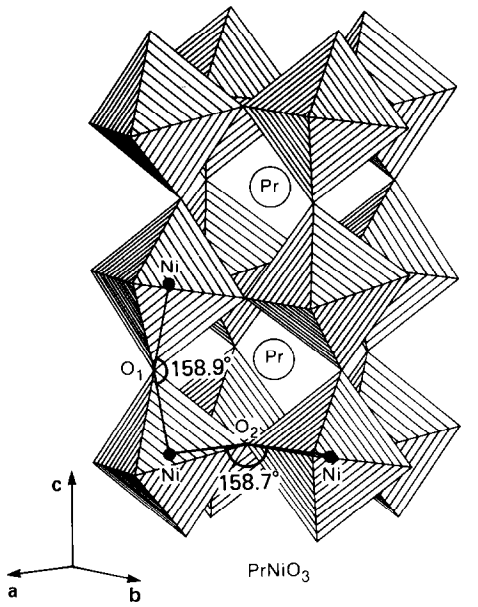

FIG. 3. Structure of $PrNiO_3$, showing NiO_6 octahedra and distortions of the Ni–O–Ni angles from 180°.

Considering the fact that no significant nonstoichiometry on any sublattice has been detected in the structural refinement of $PrNiO_3$, and given the 3+ oxidation state of praseodymium in the compound, the average formal oxidation state of nickel would most probably be Ni(III). As a matter of

TABLE III

DISTANCES (Å) AND ANGLES (°) FOR ORTHORHOMBIC $RENiO_3$ AT ROOM TEMPERATURE

	$PrNiO_3$		$NdNiO_3$	$SmNiO_3$	$HoNiO_3$[a]
	Neutron	X-ray	X-ray	X-ray	X-ray
Ni–O1 (×2)	1.938(1)	1.947(3)	1.945(4)	1.961(3)	1.919(3)
Ni–O2 (×2)	1.920(3)	1.909(11)	1.935(11)	1.943(7)	1.936(6)
Ni–O2 (×2)	1.962(2)	1.966(10)	1.949(11)	1.962(7)	1.959(6)
$\overline{Ni–O}$	1.940(2)	1.940(8)	1.943(9)	1.955(6)	1.938(5)
O1–Ni–O2	89.4(2)	91.1(7)	91.4(7)	90.8(4)	86.9(5)
O1–Ni–O2	89.4(2)	90.6(7)	90.6(7)	91.8(4)	92.3(4)
O2–Ni–O2	91.7(2)	91.6(9)	91.1(9)	90.5(6)	88.5(5)
Ni–O1–Ni	158.9(2)	156.2(5)	156.1(6)	149.4(3)	150.6(4)
Ni–O2–Ni	158.7(1)	159.9(6)	157.5(7)	154.2(4)	152.3(3)
RE–O1	2.408(7)	2.337(13)	2.340(16)	2.247(9)	2.310(12)
RE–O1	2.516(6)	2.538(9)	2.500(8)	2.404(8)	2.270(8)
RE–O1[b]	2.919(6)	2.904(9)	2.956(8)	3.151(8)	3.351(8)
RE–O1[b]	3.022(7)	3.091(13)	3.068(16)	3.138(9)	2.989(12)
RE–O2 (×2)	2.404(4)	2.430(10)	2.400(11)	2.377(7)	2.347(8)
RE–O2 (×2)	2.572(5)	2.593(10)	2.614(11)	2.514(7)	2.413(8)
RE–O2 (×2)	2.704(4)	2.689(10)	2.638(11)	2.657(7)	2.626(8)
RE–O2 (×2)[b]	3.162(4)	3.126(10)	3.189(11)	3.296(7)	3.356(8)
$(\overline{RE–O})_{8\ short}$	2.536(5)	2.537(11)	2.518(12)	2.468(8)	2.419(9)
$(\overline{RE–O})_{4\ long}$	3.066(6)	3.062(11)	3.101(12)	3.220(8)	3.263(9)
$(\overline{RE–O})$	2.712(5)	2.712(11)	2.712(12)	2.719(8)	2.700(9)

[a] From Ref. (*9*).
[b] Long *RE*–O distances.

fact, the coordination polyhedra of nickel in $PrNiO_3$, $NdNiO_3$, $SmNiO_3$, and $HoNiO_3$ are very similar and the mean Ni–O distances are almost the same (~1.94 Å). This fact would appear to indicate (*9*) that all four compounds have Ni(III) with a low spin configuration. That means that $PrNiO_3$ can be compared to the other members of the series $RENiO_3$.

Comparing the results in Tables II and III with those expected for the ideal cubic perovskite, we can see the effects of decreasing the size of the rare earth cation. This decrease appears *not* to affect the individual NiO_6 octahedra, which remain approximately octahedral with an unchanged Ni–O distance of 1.94–1.95 Å. In contrast, small rare earths strongly affect the coordination sphere around themselves. In the ideal cubic case, each *RE* has 12 equidistant neighboring oxygens. For the orthorhombically distorted structure in Tables II and III, however, the coordination polyhedron of the *RE* cation is no longer regular: the twelve oxygen neighbors become approximately split in two groups of eight short and four long distances (see Table III). In $PrNiO_3$ the difference between the mean distances to the eight nearest and to the four next nearest oxygen neighbors is about 0.5 Å, and these four next nearest neighbors participate for only 9% of the total bonding. This difference is even more pronounced when the orthorhombic distortion becomes larger. As a comparison, in $HoNiO_3$ (*9*) the difference between the mean distances of the two oxygen groups is about 0.85 Å and the four farther oxygen neighbors participate for only 4% of the total bonding.

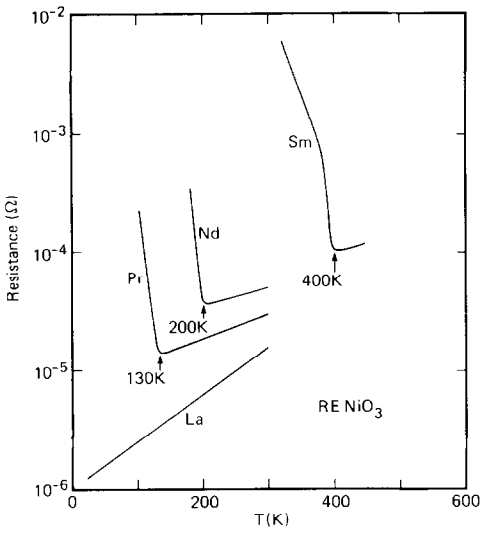

FIG. 4. Plot of log resistance versus temperature for *RE*NiO_3 showing sharp metal—insulator transitions. Since the measuring geometry is the same for different compounds, the relative resistance approximates their relative resistivity.

Physical Properties: Metal–Insulator Transition

Perhaps the most interesting physical property in these compounds is their electrical conductivity, which is summarized in Fig. 4. In accord with earlier results (*6, 9*), $LaNiO_3$ is one of the very few oxides that exhibit metallic conductivity down to 5 K. Near room temperature, the resistivities of the Pr and Nd compounds are progressively higher, but still show a metallic temperature dependence, while the resistivity of $SmNiO_3$ is much higher and semiconducting. By examining a wider temperature range (Fig. 4), we discovered metal–insulator transitions (*24*) in each of these three compounds, at which there is a sharp change in the resistivity behavior. These phase transitions are seen in conductivity measurements at 130, 200, and 400 K for Pr-, Nd-, and $SmNiO_3$, respectively. These transitions have also been seen in differential scanning calorimetry experiments in which they are shown to be clearly first order transitions near the same temperatures, with enthalpy changes of approximately 1.2, 1.6, and 2.0 J/g for the Pr, Nd, and Sm compounds, respectively. By slowly cooling through the transition and subsequently warming up, we measured the hysteresis in the transition by resistivity: ~11 K for $PrNiO_3$, but ≤2 K for the Nd and Sm compounds. (Note that the conductivity transition observed (*8*) in *RH*-$NdNiO_3$ has a much larger hysteresis (~100 K) and is much less dramatic than in *O*-$NdNiO_3$. The resistance in the former increases by a factor of ~5 over a ~100 K range, whereas the latter exhibits a change of several orders of magnitude in a ~10 K range.)

For the series of *RE*NiO_3 compounds, the temperature of the metal–insulator transition is observed to decrease (from 400 to 200 to 130 to none) as the tolerance factor increases and hence the strength of the distortion from ideal cubic perovskite decreases. Since the basic NiO_6 octahedron itself is relatively similar in these structures (Table III), the electron delocalization is then controlled by the Ni–O–Ni angle between neighboring, corner-sharing octahedra. In $HoNiO_3$ (*9*), this angle averages ~151°. As seen in Table III, it increases for Sm and Nd, reaching ~159° for Pr and higher for La, as it approaches the ideal cubic perovskite value of 180°. Thus, the increase in conducting behavior with larger *RE* shown in Fig. 4 is presumed to be associated with the increased overlap as measured by the Ni–O–Ni angle.

Low Temperature Neutron Diffraction Study

In order to find evidence for any structural or magnetic anomaly at the metal–insulator transition of $PrNiO_3$ and $NdNiO_3$, low temperature neutron thermodiffractometry was carried out on both samples. As shown in Fig. 5 for the Pr case, as the temperature is decreased toward the transition, the cell parameters exhibit a smooth thermal con-

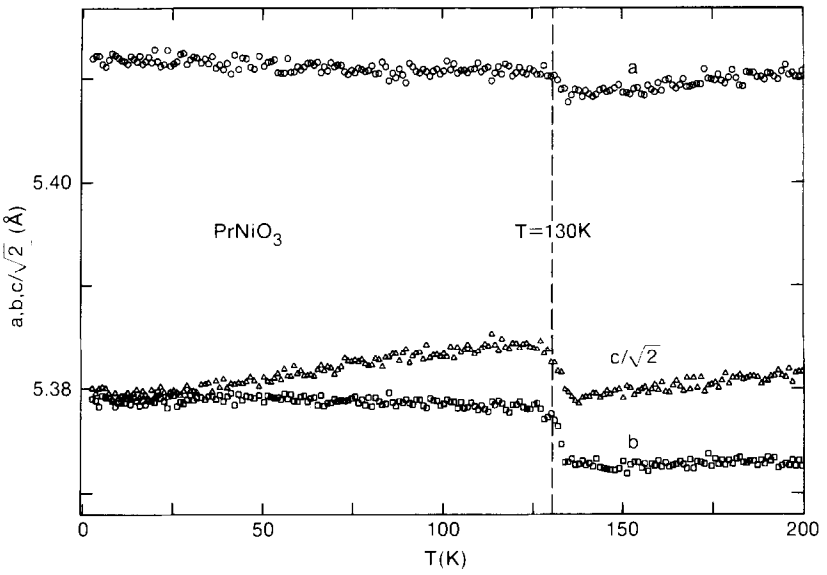

FIG. 5. Temperature dependence of lattice constants of $PrNiO_3$ showing anomalous thermal expansion upon cooling through the metal–insulator transition. Similar data were obtained for *O*-$NdNiO_3$.

traction. Cooling through the first-order metal–insulator transition, all three cell constants increase abruptly when the compounds become insulating, with the unit cell volume expanding by about 0.2%. This increase could be linked to an electronic transition on the nickel sublattice, or to an electronic localization. In addition, the transition to the insulating phase is characterized in both compounds by the appearance of new, very weak diffraction peaks that could not be indexed in the room temperature orthorhombic cell (see Fig. 6). It is not yet clear what is the origin of these new diffraction peaks. They could indicate a structural distortion (although no evidence for superstructure peaks has been found in the room temperature X-ray diffraction pattern of insulating $SmNiO_3$) and/or a magnetic ordering of Ni spins. Further experiments are needed to shed light on this point and are currently in progress.

At lower temperature and in the $NdNiO_3$ sample only, a large increase in the intensity of some of the new diffraction lines has been detected (see Fig. 6b). The evolution of one of these peaks versus temperature is shown in Fig. 7. In addition to the intensity observed below 200 K, there is a sharp rise in intensity below ~20 K. This behavior is similar to a magnetization curve typical of rare earth magnetic ordering induced by polarization and has already been encountered in other neodymium oxides (*25*). This is strong evidence in favor of magnetic ordering of the Nd^{3+} spins for $T \lesssim 20$ K. It is probable that magnetic ordering of the Ni spins at higher temperature is responsible for at least some of the additional weak peaks that appear below the metal–insulator transition. The $PrNiO_3$ sample does not exhibit the same behavior at low temperatures, indicating that the Pr sublattice does not order magnetically, consistent with the singlet ground-state of the Pr^{3+} ion.

Conclusion

A series of perovskite nickel oxides which contain rare earth cations whose ionic ra-

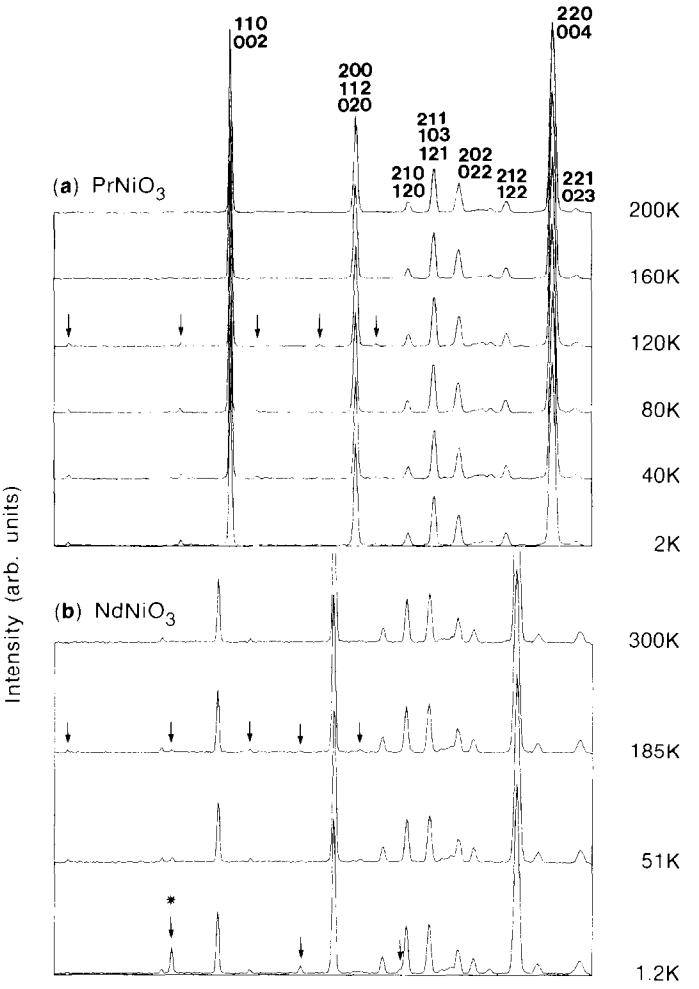

FIG. 6. Temperature dependence of the neutron scattering intensities versus scattering angle for (a) $PrNiO_3$ and (b) $NdNiO_3$, showing the new peaks which appear below the metal–insulator transition. The main peaks are indexed in space group Pbnm.

dius increases from Sm to Nd to Pr to La has been studied. By refining the structures of three of these compounds, we have shown how this increase in radius causes a decrease in the distortion of the Ni–O–Ni bond angle. Conductivity measurements reveal that these compounds have a metal–insulator transition and that increasing the rare earth radius leads to higher conductivity via decreasing the temperature of this transition. Correlating the structural and conductivity effects, we conclude that increasing the rare earth radius decreases the distortion between neighboring NiO_6 octahedra; this improves the electronic overlap between Ni ions and decreases the temperature of the metal–insulator transition. More work is needed to substantiate this correlation and understand the nature of this dramatic transition.

Acknowledgments

We thank Dr. Juan Rodriguez-Carvajal for very helpful discussions, as well as Stuart Parkin and Rich Sie-

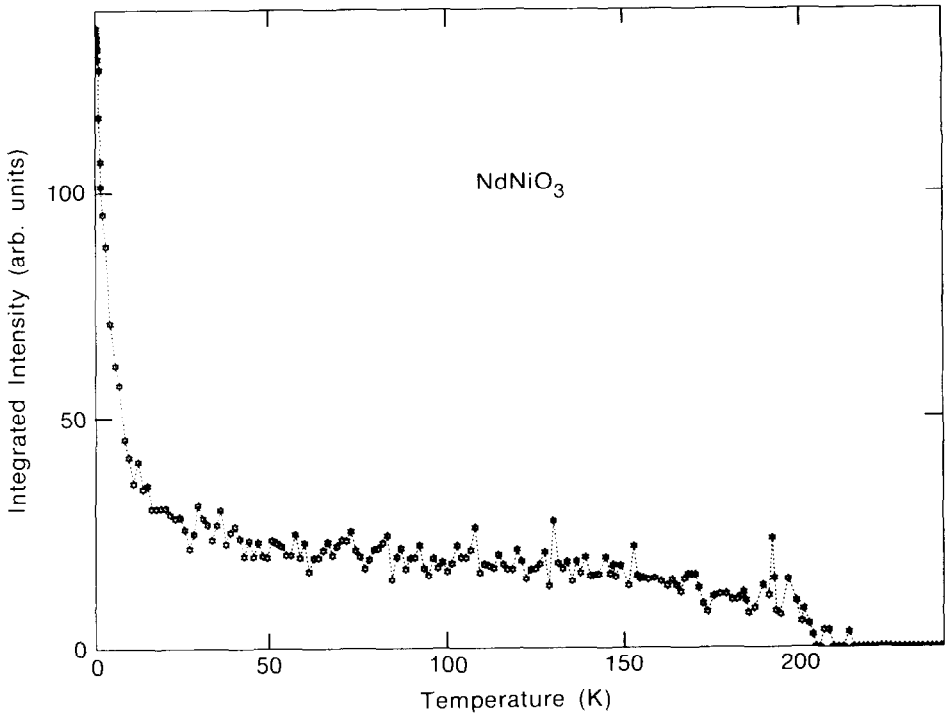

FIG. 7. Temperature dependence of the intensity of one of the weak neutron diffraction peaks of $NdNiO_3$ (indicated by a star in Fig. 6(b)).

mens for conductivity ($T > 300$ K) and DSC measurements.

Note added in proof. After this paper was submitted, we became aware of the report by Arbuckle *et al.* (*26*) of the existence of a metal–semiconudctor transition in $NdSrNiO_4$ at 190 K. This transition can probably be considered as the 2D counterpart of the metal–insulator transition observed in *O*–$NdNiO_3$ at 200 K.

References

1. A. W. SLEIGHT, J. L. GILLSON, AND F. E. BIERSTEDT, *Solid State Commun.* **17,** 27 (1975).
2. J. G. BEDNORZ AND K. A. MÜLLER, *Z. für Physik* **B64,** 189 (1986).
3. R. J. CAVA, B. BATLOGG, J. J. KRAJEWSKI, R. FARROW, AND L. W. RUPP, *Nature (London)* **332,** 814 (1988).
4. J. B. GOODENOUGH AND J. M. LONGO, "Landolt–Börnstein, Tabellen," Vol. III/4a, Springer-Verlag, Berlin (1970); S. Nomura, "Landolt–Börnstein Tabellen," Vol. III/12a, Springer-Verlag, Berlin (1978); J. B. Goodenough, *Prog. Solid State Chem.* **5,** 149 (1971).
5. J. B. TORRANCE, P. LACORRE, C. ASAVAROENGCHAI, AND R. M. METZGER, *J. Solid State Chem.*, in press.
6. J. B. GOODENOUGH AND P. M. RACCAH, *J. Appl. Phys.* **36,** 1031 (1965).
7. A. WOLD, B. POST, AND E. BANKS, *J. Amer. Chem. Soc.* **79,** 1911 (1957).
8. J. K. VASSILIOU, M. HORNBOSTEL, R. ZIEBARTH, AND F. J. DISALVO, *J. Solid State Chem.* **81,** 208 (1989).
9. G. DEMAZEAU, A. MARBEUF, M. POUCHARD, AND P. HAGENMULLER, *J. Solid State Chem.* **3,** 582 (1971).
10. A. ANTONIADIS, J. BERRUYER, AND A. FILHOL, *Acta Crystallogr. Sect. A.* **A46,** 692 (1990). A. Antoniadis, J. Berruyer, and A. Filhol, I. L. L. Internal Report 90AN08 (1990).
11. J. RODRIGUEZ-CARVAJAL, program FULLPROF, private communication.
12. H. M. RIETVELD, *J. Applied Crystallogr.* **2,** 65 (1969); D. B. Wiles and R. A. Young, *J. Applied Crystallogr.* **15,** 430 (1982).

13. S. GELLER, *J. Chem. Phys.*, **24,** 1236 (1956).
14. V. M. GOLDSCHMIDT, Geochemische Verteilungsgesetze der Elemente VII, VIII (1927/28).
15. P. POIX, *C.R. Acad. Sci. Paris* **C270,** 1852 (1970).
16. S. GELLER, *Acta Crystallogr.* **10,** 243 (1957).
17. J. S. RUIZ, A. M. ANTHONY, AND M. FOEX, *C.R. Acad. Sci. Paris* **B264,** 1271 (1967).
18. T. C. HUANG, W. PARRISH, H. TORAYA, P. LACORRE, AND J. B. TORRANCE, *Mater. Res. Bull.* **25,** 1091 (1990).
19. D. A. MACLEAN, HOK-NAM NG, AND J. E. GREEDAN, *J. Solid State Chem.* **30,** 35 (1979).
20. C. P. KHATTACK AND D. E. COX, *Mater. Res. Bull.*, **12,** 463 (1977).
21. S. GELLER, P. J. CURLANDER, AND G. F. RUSE, *Mater. Res. Bull.* **9,** 637 (1974).
22. Of course, the standard space group is *Pnma*, not *Pbnm* as adopted in the literature. However, in order to reduce confusion and facilitate comparisons with data of similar structures already in the literature, we shall use the latter.
23. I. D. BROWN, *in* "Structure and Bonding in Crystals," Vol.2, (O'Keeffe and Navrotsky Eds.), Vol. 2, p. 130, Academic Press, San Diego (1981).
24. This transition could also be called "metal–nonmetal" or "metal–semiconductor" transition, but the change in conductivity (Fig. 4) is so dramatic that we prefer the name of "metal–insulator" transition.
25. J. RODRIGUEZ-CARVAJAL, M. T. FERNANDEZ-DIAZ, J. L. MARTINEZ, F. FERNANDEZ, AND R. SAEZ-PUCHE, *Europhys. Lett.* **11,** 261 (1990).
26. B. W. ARBUCKLE, K. V. RAMANUJACHARY, Z. ZHANG, AND M. GREENBLATT, *J. Solid State Chem.* **88,** 278 (1990).